AIP | The Journal of Chemical Physics

Monolayers of hard rods on planar substrates. I. Equilibrium

M. Oettel, M. Klopotek, M. Dixit, E. Empting, T. Schilling, and H. Hansen–Goos

Citation: The Journal of Chemical Physics **145**, 074902 (2016); doi: 10.1063/1.4960618
View online: http://dx.doi.org/10.1063/1.4960618
View Table of Contents: http://scitation.aip.org/content/aip/journal/jcp/145/7?ver=pdfcov
Published by the AIP Publishing

Monolayers of hard rods on planar substrates. I. Equilibrium

M. Oettel,[1,a)] M. Klopotek,[1] M. Dixit,[2] E. Empting,[1] T. Schilling,[2] and H. Hansen–Goos[3]
[1]*Institut für Angewandte Physik, Eberhard Karls Universität Tübingen, D–72076 Tübingen, Germany*
[2]*Theory of Soft Condensed Matter, Physics and Materials Sciences Research Unit, Université du Luxembourg, L-1511 Luxembourg, Luxembourg*
[3]*Institut für Theoretische Physik, Eberhard Karls Universität Tübingen, D–72076 Tübingen, Germany*

(Received 11 May 2016; accepted 26 July 2016; published online 16 August 2016)

The equilibrium properties of hard rod monolayers are investigated in a lattice model (where position and orientation of a rod are restricted to discrete values) as well as in an off-lattice model featuring spherocylinders with continuous positional and orientational degrees of freedom. Both models are treated using density functional theory and Monte Carlo simulations. Upon increasing the density of rods in the monolayer, there is a continuous ordering of the rods along the monolayer normal ("standing up" transition). The continuous transition also persists in the case of an external potential which favors flat-lying rods in the monolayer. This behavior is found in both the lattice and the continuum models. For the lattice model, we find very good agreement between the results from the specific DFT used (lattice fundamental measure theory) and simulations. The properties of lattice fundamental measure theory are further illustrated by the phase diagrams of bulk hard rods in two and three dimensions. *Published by AIP Publishing.* [http://dx.doi.org/10.1063/1.4960618]

I. INTRODUCTION

Several systems of scientific and technological interest can be characterized as being monolayers of anisotropic particles, such as Langmuir monolayers,[1] or very thin films of elongated organic molecules,[2] such as organic semiconductors.[3,4] Since the particular molecular interactions in these systems may be very complicated, it is worthwhile to investigate simpler models of anisotropic colloids to obtain general insights into the thermal behavior of these systems. Among these, hard-body models (where particles interact only via their excluded volume) are a natural starting point to assess effects of anisotropy, both for thermal equilibrium and non-equilibrium conditions (i.e., growth of the monolayer).

We present our investigations on equilibrium and on growth of hard-rod monolayers in two papers, where in Paper I we focus on equilibrium properties and in Paper II,[30] we treat the growth process. In both papers, the focus will be on hard-rod lattice models since for these a fairly transparent theoretical analysis of equilibrium and growth is possible in the framework of density functional theory (DFT). In particular, we use the framework provided by fundamental measure theory (FMT)[5] within which very accurate density functionals for systems of anisotropic hard particles have been constructed for continuous[6] and, important for the present investigations, for lattice models.[7,8] For the subsequent investigations of the growth process, kinetic Monte Carlo (MC) simulations on a lattice are a natural starting point. Since lattice models inevitably restrict the translational and orientational degrees of freedom of rods, we will also present results for an off-lattice hard-rod (spherocylinder) model and identify similarities and differences between lattice and off-lattice models.

The restriction of orientation in hard-rod (cuboid) models comes with the benefit that density functionals become tractable and therefore also analytic results can be derived. Ref. 9 treats the phase behavior of needle-like rods in narrow slits using an Onsager-type DFT. For continuous translational degrees of freedom and in three dimensions (3D) a rich phase diagram was derived using FMT.[10] Although not all details are the same in a simulated phase diagram of hard cuboids with unrestricted orientation,[11] the restricted-orientation model gives a good first estimate of what can be expected. If the particles are restricted to a plane (the monolayer case), the first-order isotropic-nematic transition becomes a continuous one, according to FMT in the restricted-orientation model.[12,13] The orientational order perpendicular to the plane Q is proportional to the density ρ for low densities. An approximate DFT and simulations for hard ellipsoids (unrestricted orientation) seem to confirm this behavior although very low densities have not been sampled in the simulations.[14] Such a possible qualitative change of the nature of the nematic transition through dimensional restriction is very interesting by itself, and therefore we will establish analytically the $Q \propto \rho$ behavior explicitly in the low-density limit for both lattice and continuum models. The presence of an orientation-dependent external potential in the monolayer plane (substrate potential) does not change the continuous nature of the nematic transition but the onset of particles "standing up" may become very sharp for substrate potentials which actually favor particles "lying down."

The structure of the paper is as follows: In Sec. II, we describe the lattice version of fundamental measure theory (FMT) for hard rod mixtures and give illustrative examples for the functionals. The bulk equilibrium properties of monocomponent rods in two dimensions (2D) and three dimensions (3D) are briefly discussed, followed by the results

a)martin.oettel@uni-tuebingen.de

for the monolayer (3D confined). Sec. III discusses the spherocylinder off-lattice model for the monolayer using DFT in the low-density limit and using simulations. Sec. IV discusses similarities and differences between the lattice and off-lattice models and gives a summary. Two appendices briefly discuss the grand canonical simulation method for the lattice model and the derivation of the excluded area between hard rods (in the continuum model) whose centers are confined to a plane.

II. DENSITY FUNCTIONAL THEORY FOR HARD ROD LATTICE MODELS

A. Fundamental measure theory

The rod model used in this work is formulated on a simple cubic lattice in d dimensions. A lattice point $\mathbf{s}$ is specified by a set of d integers ($\mathbf{s} = (s_1, \ldots, s_d)$). The lattice constant a is the unit of length. Hard rods are lines (1D), rectangles (2D), or parallelepipeds (3D) with corners sitting on lattice points, and thus their geometry is specified by their extent in the cartesian directions, which are again sets of d integers. The position of a rod is specified by the corner whose lattice coordinates are minimal each (see Fig. 1). Hard rods are not allowed to overlap (but they may "touch," i.e., share surfaces), thus the interaction potential for two rods $\mathcal{L}_i$ and $\mathcal{L}_j$ of species i and j at positions $\mathbf{s}_i$ and $\mathbf{s}_j$ with extensions $\mathbf{L}_i = (L_{i,1}, \ldots, L_{i,d})$ and $\mathbf{L}_j = (L_{j,1}, \ldots, L_{j,d})$ is given by

$$u_{ij}(\mathbf{s}_i, \mathbf{s}_j) = \begin{cases} \infty & (f_{ij} = 1) \\ 0 & (f_{ij} = 0) \end{cases}. \tag{1}$$

Here, $f_{ij} = f(\mathbf{s}_i, \mathbf{s}_j, \mathbf{L}_i, \mathbf{L}_j)$ is the rod overlap function given by

$$f(\mathbf{s}_i, \mathbf{s}_j, \mathbf{L}_i, \mathbf{L}_j) = \prod_{k=1}^{d} \theta(s_{i,k}, s_{j,k}, L_{i,k}, L_{j,k}), \tag{2}$$

$$\theta(s_{i,k}, s_{j,k}, L_{i,k}, L_{j,k}) = \begin{cases} 1 & (s_{j,k} = \{s_{i,k} - (L_{j,k} - 1), \ldots, s_{i,k} + (L_{i,k} - 1)\}) \\ 0 & (\text{otherwise}) \end{cases}. \tag{3}$$

The overlap function is 1 whenever there is an overlap in all lattice dimensions, meaning that the rods are disjunct for $f = 0$ (see Fig. 1). Note that due to the chosen convention for the rod location the overlap function is not symmetric in the rod locations $\mathbf{s}_i$ and $\mathbf{s}_j$.

In the following we consider such a rod mixture with ν species subject to external fields $V^{\text{ext}}(\mathbf{s}) = \{V_1^{\text{ext}}(\mathbf{s}), \ldots, V_\nu^{\text{ext}}(\mathbf{s})\}$ where $V_j^{\text{ext}}(\mathbf{s})$ acts on rod species j. At lattice site $\mathbf{s}$, the number density of rods per lattice site is specified by $\rho(\mathbf{s}) = \{\rho_1(\mathbf{s}), \ldots, \rho_\nu(\mathbf{s})\}$, where $\rho_j(\mathbf{s})$ is the density of rod species j, i.e., the probability of a given site to be occupied by the lower left corner of a particle. In density functional theory, all equilibrium properties of a rod mixture in external fields are obtained by minimizing the grand potential functional,

$$\Omega[\rho(\mathbf{s})] = \mathcal{F}^{\text{id}}[\rho(\mathbf{s})] + \mathcal{F}^{\text{ex}}[\rho(\mathbf{s})] - \sum_{i=1}^{\nu} \sum_{\mathbf{s}} (\mu_i - V_i^{\text{ext}}(\mathbf{s}))\, \rho_i(\mathbf{s}), \tag{4}$$

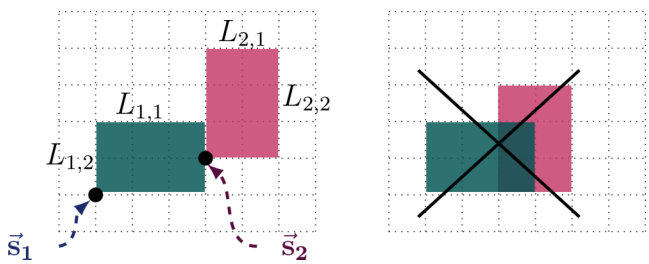

FIG. 1. Definitions for the example of hard 2×3-rods in $d = 2$. Rod location is specified by the position of the lower left corner (i.e., the corner whose lattice coordinates are minimal). Rods may "touch" (left) but not overlap (right).

with respect to the particle densities $\rho(\mathbf{s})$. The chemical potential for rod species $i = 1 \ldots \nu$ is denoted by μ_i. If different species belong to the same type of rod in different orientations, the corresponding chemical potentials must be equal in equilibrium. $\mathcal{F}^{\text{id}}[\rho(\mathbf{s})]$ denotes the ideal gas contribution to the free energy functional, given by

$$\mathcal{F}^{\text{id}}[\rho(\mathbf{s})] = \sum_{i=1}^{\nu} \sum_{\mathbf{s}} \rho_i(\mathbf{s})(\ln \rho_i(\mathbf{s}) - 1). \tag{5}$$

Energies are measured in units of $k_B T$ throughout the paper.

The exact form of the excess free energy functional $\mathcal{F}^{\text{ex}}$ is in general unknown, and in this work we will approximate it within the fundamental measure approach. For lattice models of hard rods, this approach has been worked out in Refs. 7 and 8, resulting in an approximative form for $\mathcal{F}^{\text{ex}}$ which we apply in the present study (Lafuente–Cuesta functional).

The class of free energy functionals derived in Refs. 7 and 8 makes use of weighted densities $n^\alpha(\mathbf{s})$, which are defined as convolutions of densities $\rho(\mathbf{s})$ with weight functions $w^\alpha := \{w_1^\alpha, \ldots, w_\nu^\alpha\}$,

$$n^\alpha(\mathbf{s}) = \sum_{i=1}^{\nu} \rho_i \otimes w_i^\alpha(\mathbf{s}). \tag{6}$$

Convolutions ($\otimes$) on the lattice are defined as

$$(f \otimes g)(\mathbf{s}) = \sum_{\mathbf{s}'} f(\mathbf{s}') g(\mathbf{s} - \mathbf{s}'). \tag{7}$$

The d-dimensional index $\alpha = (\alpha_1, \ldots, \alpha_d)$ specifies different weight functions w_i^α, with allowed values $\alpha_i = 0, 1$ only. The weight functions w_i^α (specific for species i) have the meaning of defining a support of rods $\mathcal{K}_i^\alpha$ with edge lengths

$\mathbf{K}_i^\alpha = (K_{i,1}^{\alpha_1}, \ldots, K_{i,d}^{\alpha_d})$, i.e., they are 1 on points covered by $\mathcal{K}_i^\alpha$ and 0 otherwise. This can be formalized using the θ-function already employed for defining rod overlap (Eq. (3)),

$$w_i^\alpha(\mathbf{s}) = \prod_{k=1}^{d} \theta(0, s_k, \alpha_k, K_{i,k}^1). \tag{8}$$

The edge lengths of rods $\mathcal{K}_i^\alpha$ are related to those of the rods $\mathcal{L}_i$ as follows:

$$K_{i,k}^{\alpha_k} = L_{i,k} - (1 - \alpha_k) \qquad (k = 1, \ldots, d), \tag{9}$$

i.e., whenever the index α_j is 0, the edge length of $\mathcal{K}_i^{\alpha_i}$ in the dimension j is shortened by 1 compared to the corresponding edge length of $\mathcal{L}_i$, otherwise ($\alpha_j = 1$) the edge length is identical. In particular, for $\alpha = (1, \ldots, 1)$ all rods $\mathcal{K}_i^{\alpha_i}$ are identical to $\mathcal{L}_i$. The meaning of the corresponding weighted density $n^{(1,\ldots,1)}(\mathbf{s}) = \eta(\mathbf{s})$ is a local packing or volume fraction of rods at point $\mathbf{s}$. Fig. 2 illustrates the four possible weight functions for a rod with edge lengths $\mathbf{L} = (3,2)$ on a 2D lattice.

As a second ingredient, the Lafuente–Cuesta functional needs the excess free energy of a zero-dimensional (0d) cavity, Φ^{0d}, i.e., a restricted domain on the lattice which can only hold one particle at a time. Such a cavity may consist of more than one point where the rod is positioned. Furthermore, for a mixture, the set of points $\{s_{\mathrm{cav},i}\}$ specifying the allowed location of species i does not need to coincide with the corresponding set $\{s_{\mathrm{cav},j}\}$ for species j. Note that the sets $\{s_{\mathrm{cav},i}\}$ and $\{s_{\mathrm{cav},j}\}$ are not independent since the 0D cavity property is required to hold globally for the mixture, and not just for the individual components. The free energy $\Phi^{0d}(\eta)$ of such a cavity is a function exclusively of the total packing fraction $\eta \equiv \eta_{\mathrm{cav}} = \sum_{i=1}^{\nu} \sum_{\mathbf{s} \in \{s_{\mathrm{cav},i}\}} \rho_i(\mathbf{s})$ in the cavity,

$$\Phi^{0d}(\eta) = \eta + (1 - \eta)\ln(1 - \eta). \tag{10}$$

Using this 0d free energy, the Lafuente–Cuesta excess free energy functional is given by

$$\mathcal{F}^{\mathrm{ex}} = \sum_{\mathbf{s}} \mathcal{D}_\alpha \Phi^{0d}(n^\alpha(\mathbf{s})). \tag{11}$$

Remember that α is a d-dimensional index with entries $\{0,1\}$ only. In Eq. (11), $\mathcal{D}_\alpha = \prod_{i=1}^{d} D_{\alpha_i}$ and D_{α_i} is the difference operator acting on a function $f(\alpha_i)$ according to $D_{\alpha_i} f(\alpha_i) = f(1) - f(0)$.

It can be shown that $\mathcal{F}^{\mathrm{ex}}$ as defined above yields the correct excess free energy, Eq. (10), for *any* 0D cavity.[7,8] In order to assess the accuracy of the expression for situations of less severe confinement, we explicitly evaluate the properties of different bulk systems in Sec. II C. In a first step, however, we illustrate the construction of the Lafuente–Cuesta functional by applying it to different mixtures in 1D, 2D, and 3D.

B. Special cases

Here we give the explicit functionals for some special mixtures. The equilibrium properties of examples (b) and (c) (2D and 3D systems) will be discussed in Sec. II C and those of example (d) (monolayer) in Sec. II D.

(a) $d = 1$: Mixture of hard rods in one dimension. The excess free energy functional is given by

$$\mathcal{F}^{\mathrm{ex}} = \sum_{\mathbf{s}} \left(\Phi^{0d}(n^{(1)}(\mathbf{s})) - \Phi^{0d}(n^{(0)}(\mathbf{s})) \right). \tag{12}$$

This is the well-known exact solution for the 1d lattice hard rod mixture, derived in Ref. 7 following the recipe from Ref. 15 which treats the 1D continuum hard rod mixture. Another yet different derivation can be found in Ref. 16.

(b) $d = 2$: A system of rods with length L and width 1 corresponds to the binary mixture with rod lengths $\mathbf{L}_1 = (L,1)$ and $\mathbf{L}_2 = (1,L)$. The excess free energy functional is given by

$$\mathcal{F}^{\mathrm{ex}} = \sum_{\mathbf{s}} \Big(\Phi^{0d}(n^{(1,1)}(\mathbf{s})) - \Phi^{0d}(n^{(0,1)}(\mathbf{s})) - \Phi^{0d}(n^{(1,0)}(\mathbf{s})) \Big). \tag{13}$$

The weighted densities are given by

$$\begin{aligned} n^{(1,1)}(\mathbf{s}) &= \rho_1 \otimes w_1^{(1,1)}(\mathbf{s}) + \rho_2 \otimes w_2^{(1,1)}(\mathbf{s}), \\ n^{(0,1)}(\mathbf{s}) &= \rho_1 \otimes w_1^{(0,1)}(\mathbf{s}), \\ n^{(1,0)}(\mathbf{s}) &= \rho_2 \otimes w_2^{(1,0)}(\mathbf{s}). \end{aligned} \tag{14}$$

Note that the weights $w_2^{(0,1)} = w_1^{(1,0)} = 0$ since they correspond to the support of rods with width 0. Likewise $w_1^{(0,0)} = w_2^{(0,0)} = 0$.

(c) $d = 3$: A system of rods with length L and height/width 1 corresponds to the ternary mixture with rod lengths $\mathbf{L}_1 = (L,1,1)$, $\mathbf{L}_2 = (1,L,1)$ and $\mathbf{L}_3 = (1,1,L)$. The excess free energy functional is given by

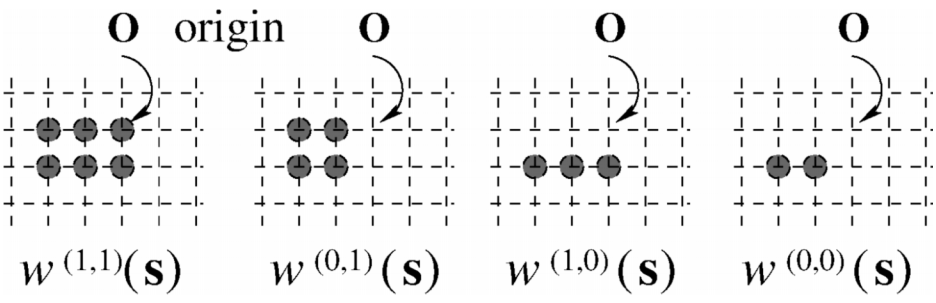

FIG. 2. The four FMT weight functions for a rod with edge lengths $\mathbf{L} = (3,2)$. The lattice point at which the weight functions are evaluated is denoted by $\mathbf{s}$. The thick points indicate on which lattice points the weight function is 1.

$$\mathcal{F}^{\mathrm{ex}} = \sum_{\mathbf{s}} \left(\Phi^{0d}(n^{(1,1,1)}(\mathbf{s})) - \Phi^{0d}(n^{(0,1,1)}(\mathbf{s})) - \Phi^{0d}(n^{(1,0,1)}(\mathbf{s})) - \Phi^{0d}(n^{(1,1,0)}(\mathbf{s})) \right). \tag{15}$$

The weighted densities are given by

$$\begin{aligned} n^{(1,1,1)}(\mathbf{s}) &= \rho_1 \otimes w_1^{(1,1,1)}(\mathbf{s}) + \rho_2 \otimes w_2^{(1,1,1)}(\mathbf{s}) \\ &\quad + \rho_3 \otimes w_3^{(1,1,1)}(\mathbf{s}), \end{aligned} \tag{16}$$

$$\begin{aligned} n^{(0,1,1)}(\mathbf{s}) &= \rho_1 \otimes w_1^{(0,1,1)}(\mathbf{s}), \\ n^{(1,0,1)}(\mathbf{s}) &= \rho_2 \otimes w_2^{(1,0,1)}(\mathbf{s}), \\ n^{(1,1,0)}(\mathbf{s}) &= \rho_3 \otimes w_3^{(1,1,0)}(\mathbf{s}). \end{aligned} \tag{17}$$

Similarly to case (b), the weights $w_i^{(\alpha_1,\alpha_2,\alpha_3)} = 0$ whenever $\alpha_j = 0$ and $i \neq j$ since they correspond to the support of rods with width 0.

(d) $d = 3$ (confined), the monolayer: A system of rods with length L and height/width 1 whose positions are constrained to a 2D-plane corresponds to a 2D ternary mixture with rod lengths $\mathbf{L}_1 = (L, 1)$, $\mathbf{L}_2 = (1, L)$ (rods lying in-plane), and $\mathbf{L}_3 = (1, 1)$ (rods standing up). The excess free energy functional is given by formally the same functional as in (a),

$$\begin{aligned} \mathcal{F}^{\mathrm{ex}} = \sum_{\mathbf{s}} \Big(& \Phi^{0d}(n^{(1,1)}(\mathbf{s})) \\ & - \Phi^{0d}(n^{(0,1)}(\mathbf{s})) - \Phi^{0d}(n^{(1,0)}(\mathbf{s})) \Big), \end{aligned} \tag{18}$$

but now the weighted densities are given by

$$\begin{aligned} n^{(1,1)}(\mathbf{s}) &= \rho_1 \otimes w_1^{(1,1)}(\mathbf{s}) + \rho_2 \otimes w_2^{(1,1)}(\mathbf{s}) \\ &\quad + \rho_3 \otimes w_3^{(1,1)}(\mathbf{s}), \\ n^{(0,1)}(\mathbf{s}) &= \rho_1 \otimes w_1^{(0,1)}(\mathbf{s}), \\ n^{(1,0)}(\mathbf{s}) &= \rho_2 \otimes w_2^{(1,0)}(\mathbf{s}). \end{aligned} \tag{19}$$

C. Equilibrium bulk properties in 2D and 3D

1. $d = 2$, the binary mixture with rod lengths $\mathbf{L}_1 = (L, 1)$ and $\mathbf{L}_2 = (1, L)$

In the bulk, both densities (ρ_1 and ρ_2) and all weighted densities are constant. We introduce the total density $\rho := \rho_1 + \rho_2$ and denote by $\eta := n^{(1,1)} = L\rho$ the total packing fraction. Furthermore $n^{(0,1)} = (L-1)\rho_1$, $n^{(1,0)} = (L-1)\rho_2$, and $S = (\rho_1 - \rho_2)/\rho$ is an order parameter for the demixed state. We refrain from calling S a nematic order parameter, since the alignment of rods corresponds just to a demixed state between species 1 and 2, and the corresponding transition has the character of a liquid–vapor transition.[17] The bulk free energy density, $f_{2d}(\rho, S) = f_{2d}^{\mathrm{id}} + f_{2d}^{\mathrm{ex}}$, written as depending on the variables ρ and S becomes

$$f_{2d}^{\mathrm{id}} = \sum_{i=1}^{3} \rho_i \ln \rho_i - \rho, \tag{20}$$

$$f_{2d}^{\mathrm{ex}} = \Phi^{0d}(\rho L) - \Phi^{0d}((L-1)\rho_1) - \Phi^{0d}((L-1)\rho_2), \tag{21}$$

$$\rho_1 = \frac{\rho}{2}(1+S), \tag{22}$$

$$\rho_2 = \frac{\rho}{2}(1-S). \tag{23}$$

At fixed ρ, the equilibrium demixing parameter S_{eq} is found by solving $\mu_S = \partial f_{2d}/\partial S = 0$. For $L \leq 3$, the mixed state ($S_{\mathrm{eq}} = 0$) is the only solution and f is minimal there. For $L \geq 4$ there exists a critical packing fraction $\eta_c < 1$ above which three solutions $S = \{0, \pm S_{\mathrm{eq}}\}$ signal demixing: the solutions $S \neq 0$ have lower free energy. At η_c, there is no jump in the demixing parameter, which is the behavior also observed at a liquid–vapor transition. One may thus expand

$$\mu_S(\eta, S) \approx \mu_{1,S}(\eta) S + \mu_{3,S}(\eta) S^3 + \cdots \tag{24}$$

and find the critical packing fraction by solving $\mu_{1,S}(\eta_c) = 0$, with the solution

$$\eta_c = \frac{2}{L-1}. \tag{25}$$

The equilibrium demixing $S_{\mathrm{eq}}(\eta)$ in the vicinity of η_c can be approximated by solving $\mu_S = 0$ for S using the Taylor approximation (24), giving

$$S_{\mathrm{eq}} = \sqrt{-\frac{\mu_{1,S}(\eta)}{\mu_{3,S}(\eta)}} \approx \sqrt{\eta - \eta_c} \sqrt{\frac{3}{2(L-2)}} (L-1). \tag{26}$$

The behavior of $S_{\mathrm{eq}}(\eta)$ near η_c born out by the approximate theory is, of course, of mean-field type.

These findings can be compared with simulation work which finds the demixing transition for $L \geq 7$[18,19] and a critical packing fraction $\eta_c \approx 5/L$.[20] Thus, FMT overestimates the tendency to demix. Note, however, that the demixing follows from a *single* functional, unlike other approaches which assume distinct expressions for the isotropic and the demixed phase free energies.[20] For very high packing fractions $\eta \approx 1$, theoretical arguments predict a reentrant transitions from the demixed to a disordered state, bearing some characteristics of a cubatic phase on a lattice.[18] This transition has been studied in more detail using simulations in Refs. 21 and 22. The present FMT functional, however, does not give this transition. For rods with extensions $m \times mL$ (where m, mL are integer and L may be noninteger), the phase diagram has been investigated in Refs. 23 and 24 where (for $m > 1$) it is shown that a columnar phase appears between the demixed and high-density disordered phase.

In 2D continuum models with anisotropic particles, simulations have frequently addressed the case of hard ellipses. A recent work finds a critical aspect ratio of $L_c \lesssim 4$.[25]

2. $d = 3$, the ternary mixture with rod lengths $\mathbf{L}_1 = (L,1,1)$, $\mathbf{L}_2 = (1,L,1)$, and $\mathbf{L}_3 = (1,1,L)$

The total density is $\rho = \rho_1 + \rho_2 + \rho_3$ and the total packing fraction is $\eta := n^{(1,1,1)} = L\rho$. We define the order parameters

$$\begin{aligned} Q &= \frac{\rho_3 - \frac{\rho_1+\rho_2}{2}}{\rho_1+\rho_2+\rho_3}, \\ S &= \frac{\rho_1 - \rho_2}{\rho_1+\rho_2}. \end{aligned} \tag{27}$$

$Q \neq 0$ signifies an excess ($Q > 0$) or depletion ($Q < 0$) of particles in z-direction (nematic state) while $S \neq 0$ signals order in the x–y–plane orthogonal to the nematic director (biaxial state). The bulk free energy density, $f_{3d}(\rho,Q,S) = f_{3d}^{\mathrm{id}} + f_{3d}^{\mathrm{ex}}$, written in dependence on the variables ρ, Q, and S becomes

$$f_{3d}^{\mathrm{id}} = \sum_{i=1}^{3} \rho_i \ln \rho_i - \rho, \tag{28}$$

$$f_{3d}^{\mathrm{ex}} = \Phi^{0d}(L\rho) - \Phi^{0d}((L-1)\rho_1) - \Phi^{0d}((L-1)\rho_2) - \Phi^{0d}((L-1)\rho_3), \tag{29}$$

$$\rho_1 = \frac{\rho}{3}(1-Q)(1+S), \tag{30}$$

$$\rho_2 = \frac{\rho}{3}(1-Q)(1-S), \tag{31}$$

$$\rho_3 = \frac{\rho}{3}(1+2Q). \tag{32}$$

Minimization of the total free energy density with respect to Q and S shows that the model has a stable nematic state ($Q = Q_{\min} > 0$, $S = 0$) for $L \geq 4$. Note that the director could also be oriented along the x- or y-axis instead of the chosen z-axis. A pure nematic state with director along the $x[y]$-axis and order parameter Q' is equivalent to a minimum free energy state with $Q = -Q'/2$ and $S = \pm 3Q'/(2+Q')$ using the order parameters (27). This is therefore not a biaxial state. The associated liquid-nematic transition is of first order, and we have determined coexistence between the liquid and the nematic state by performing the common tangent construction for the free energy density $f_{3d}(\rho,0,0)$ (liquid phase) and $f_{3d}(\rho,Q_{\min},0)$ (nematic phase), which implies equality of the chemical potential $\mu = (\partial f_{3d})/(\partial\rho)$ and pressure $p = \mu\rho - f_{3d}$. Results are shown in Fig. 3(b).

The packing fractions of the coexisting nematic state are very well described by $\eta_{\mathrm{c,nem}} = 3.58/L$. The gap in packing fractions of the coexisting states has a maximum of ≈ 0.08 at $L = 8$ and tends to zero as $L \to \infty$.

We have not found any simulation data for the 3D lattice rods to compare with. On the other hand, our FMT results are qualitatively similar to findings for 3D hard rods in the continuum. For hard spherocylinders, the isotropic-nematic transition sets in for aspect ratios larger than approximately 3.7. The transition is a clear first-order transition with a maximum in the coexistence gap at an aspect ratio of about 10.[26]

D. The monolayer system

In the lattice model, this is the effectively 2D ternary mixture with rod lengths $\mathbf{L}_1 = (L,1)$, $\mathbf{L}_2 = (1,L)$ (rods lying in-plane) and $\mathbf{L}_3 = (1,1)$ (rods standing up).

The total density is $\rho = \rho_1 + \rho_2 + \rho_3$ and the total packing fraction in the plane is $\eta := n^{(1,1)} = L(\rho_1+\rho_2) + \rho_3$. The order parameters Q and S are the same as in Eqs. (27). $Q > 0$ signifies an excess of particles "standing-up" (nematic state) while $S \neq 0$ signals demixing of "lying-down" particles (biaxial state, if additionally $Q \neq 0$). In the bulk free energy density, $f_{3d,\mathrm{conf}}(\rho,Q,S) = f_{3d,\mathrm{conf}}^{\mathrm{id}} + f_{3d,\mathrm{conf}}^{\mathrm{ex}}$, one can identify $f_{3d,\mathrm{conf}}^{\mathrm{id}} = f_{3d}^{\mathrm{id}}$ whereas the excess part becomes

$$f_{3d,\mathrm{conf}}^{\mathrm{ex}} = \Phi^{0d}(L(\rho_1+\rho_2)+\rho_3) - \Phi^{0d}((L-1)\rho_1) - \Phi^{0d}((L-1)\rho_2). \tag{33}$$

At fixed total density ρ, the minimization of the free energy with respect to Q and S reveals the following picture: For "small" rod lengths $L \leq 12$ there is no biaxial state ($S = 0$, no demixing in the plane), but the "nematic" order parameter Q grows monotonically and smoothly from 0 to 1 when the total density varies between 0 and 1 (close-packed state of rods standing up). Results for $L = 4 \ldots 10$ are shown in Fig. 4(a), demonstrating that for increasing L the rods quickly "stand up." The FMT results show excellent agreement with Monte Carlo simulation results[27] on the same confined model for $L = 4$ and 6. For larger rod lengths ($L = 8$ and 10) the agreement with our grand canonical Monte Carlo (GCMC)

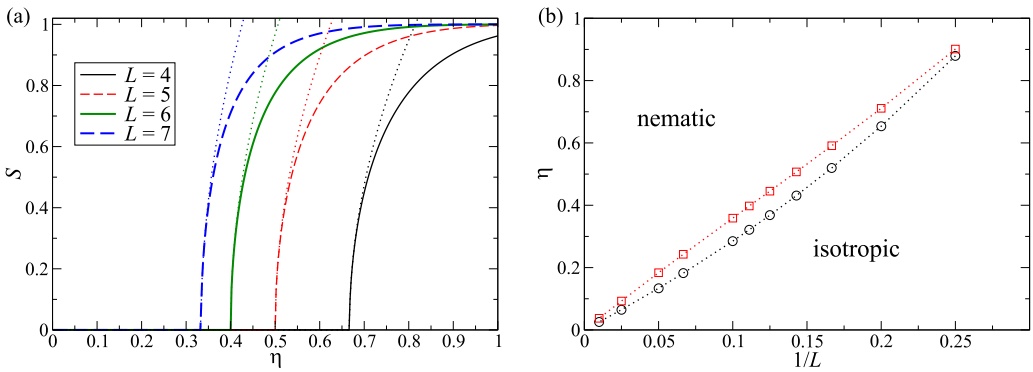

FIG. 3. (a) Rods in $d = 2$: Demixing order parameter S as a function of the total packing fraction for different rod lengths L. Dotted lines correspond to the approximate solution near the onset of demixing (Eq. (26)). (b) Rods in $d = 3$. Liquid–nematic binodal in the plane spanned by the inverse rod length $1/L$ and the packing fraction η. Square symbols show the packing fraction of the coexisting nematic state, circles the packing fraction of the coexisting liquid state.

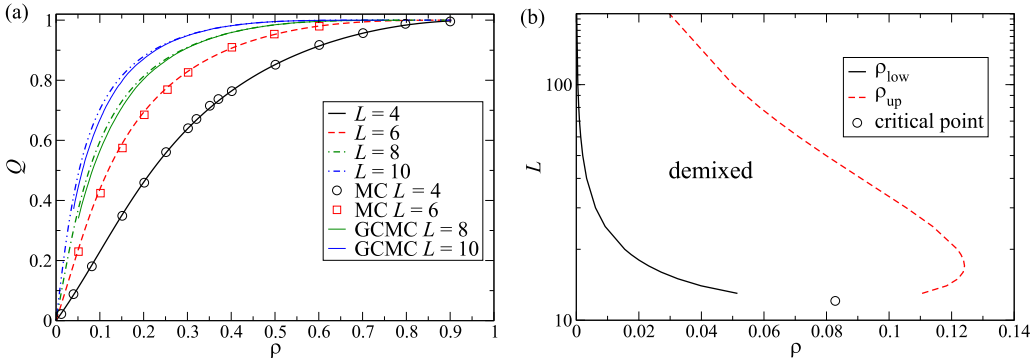

FIG. 4. (a) Order parameter Q for rods standing up vs. total density. Lines are results from FMT and symbols are results from Monte Carlo simulations reported in Ref. 27. Thin lines are results from our GCMC simulations where a running average of 20 points on density intervals of 0.04 has been taken. (b) Phase diagram from FMT showing a reentrant behavior for mixing ($S = 0$) and demixing ($S \neq 0$) in the plane. The rod length L is treated as a continuous variable. The critical point occurs for a rod length of $L_c \approx 12.077$ at a density of $\rho_c \approx 0.0828$.

simulations is only slightly worse. The implementation of GCMC is briefly described in Appendix A.

For $L \geq 13$, FMT predicts reentrant demixing in the plane, i.e., in a certain interval $[\rho_{\text{low}}(L), \rho_{\text{up}}(L)]$ for the total density the biaxiality parameter will be nonzero, $S \neq 0$. This reentrant behavior is qualitatively understood as follows. In the $d = 2$ model it was found that the critical density of demixing of planar rods is $\rho_1 + \rho_2 = 2/(L(L-1))$. For increasing L one therefore expects $\rho_{\text{low}}(L) \to 0$. On the other hand, for a certain L but increasing ρ the fraction of planar rods initially grows, reaches a maximum, and becomes smaller again since the rods stand up, see Fig. 4(a). Therefore, if there exists a lower demixing density $\rho_{\text{low}}(L)$, one would expect the existence of a higher remixing density $\rho_{\text{up}}(L)$ owing to the reduction of the planar rod density. Similarly as in the $d = 2$ model, the demixing transition is continuous and hence the densities $\rho_{\text{low}}(L), \rho_{\text{up}}(L)$ can be found using the following argument: Let $\mu_Q(\rho, Q, S) = \partial f_{3d,\text{conf}}/\partial Q$ and $\mu_S(\rho, Q, S) = \partial f_{3d,\text{conf}}/\partial S$ be chemical potentials for the order parameters Q and S. For a mixed state ($S = 0$), we define $Q_{\text{eq}}(\rho)$ through $\mu_Q(\rho, Q_{\text{eq}}, 0) = 0$. As before, we may expand

$$\mu_S(\rho, Q, S) \approx \mu_{1,S}(\rho, Q)S + \mu_{3,S}(\rho, Q)S^3 + \cdots. \quad (34)$$

At the de-/remixing densities one has the condition

$$\mu_{1,S}(\rho, Q_{\text{eq}}(\rho))|_{\rho=\rho_{\text{low[up]}}} = 0, \quad (35)$$

which needs to be solved numerically. The results are depicted in Fig. 4(b), showing the onset of demixing at $L = 13$ and a maximum density interval for the demixed state at around $L = 20$.

The continuous behavior of $Q(\rho)$ and the reentrant demixing are in fact very similar to the behavior found in the FMT study of the restricted-orientation model with continuous translational degrees of freedom.[12] There, biaxial ordering sets in at larger rod lengths, $L \geq 21.34$.

The results in Fig. 4 suggest $Q \propto \rho$, i.e., the continuous nematic ordering sets in at $\rho = 0$. This is easily understood in a low-density expansion of the FMT excess free energy (33) which is exact up to second order. Assuming no biaxiality ($S = 0$) and combining ideal and excess part we find for the free energy derivative with respect to Q,

$$\mu_Q = \frac{\partial f_{3d,\text{conf}}}{\partial Q} \approx \frac{2}{3}\rho \ln \frac{1+2Q}{1-Q} + \frac{2}{9}\rho^2\left([2 - L - L^2] + [L-1]^2 Q\right) + O(\rho^3). \quad (36)$$

Note that in the excess part of μ_Q, at fixed density, there is a constant term driving the system to $Q > 0$ for $L \geq 2$. This is different from the 2D and 3D bulk systems where this constant term is absent and thus $Q > 0$ (for low densities) is always unfavorable in terms of free energy cost. The equilibrium solution $\mu_Q = 0$ at $Q = Q_{\text{eq}}$ is found as

$$\rho = \frac{3 \ln \frac{1+2Q_{\text{eq}}}{1-Q_{\text{eq}}}}{[L^2 + L - 2] - [L-1]^2 Q_{\text{eq}}} \to Q_{\text{eq}} \approx \frac{1}{9}(L^2 + L - 2)\rho. \quad (37)$$

Hence, for large L the lattice model predicts the scaling $Q_{\text{eq}} \propto \rho L^2$.

1. *Finite substrate potential*

One may ask whether a finite substrate potential could alter the continuous transition found above. It is natural to assume that the substrate potential acts equally on the flat-lying species 1 and 2 and differently on the upright species 3. Hence the external contribution to the free energy becomes

$$f^{\text{ext}} = \sum_{i=1}^{3} V_i^{\text{ext}} \rho_i = v_0(\rho_1 + \rho_2) + v_3\rho_3 = \frac{\rho}{3}(2v_0 + v_3) + \frac{2}{3}\rho Q(v_3 - v_0). \quad (38)$$

Therefore the free energy derivative with respect to Q is modified as $\mu_Q \to \mu_Q + \rho v_Q$ with $v_Q = \frac{2}{3}(v_3 - v_0)$. For the ideal gas limit this implies an initial ordering on the substrate with order parameter

$$Q_{\text{id}} = \frac{\exp(-3v_Q/2) - 1}{\exp(-3v_Q/2) + 2}. \quad (39)$$

If the substrate is strongly attractive for the flat-lying species 1 and 2 ($v_Q \gg 0$), then we find $Q_{\text{id}} \to -1/2$. At nonzero densities, the solution of $\mu_Q = 0$ (Eq. (36) with the external

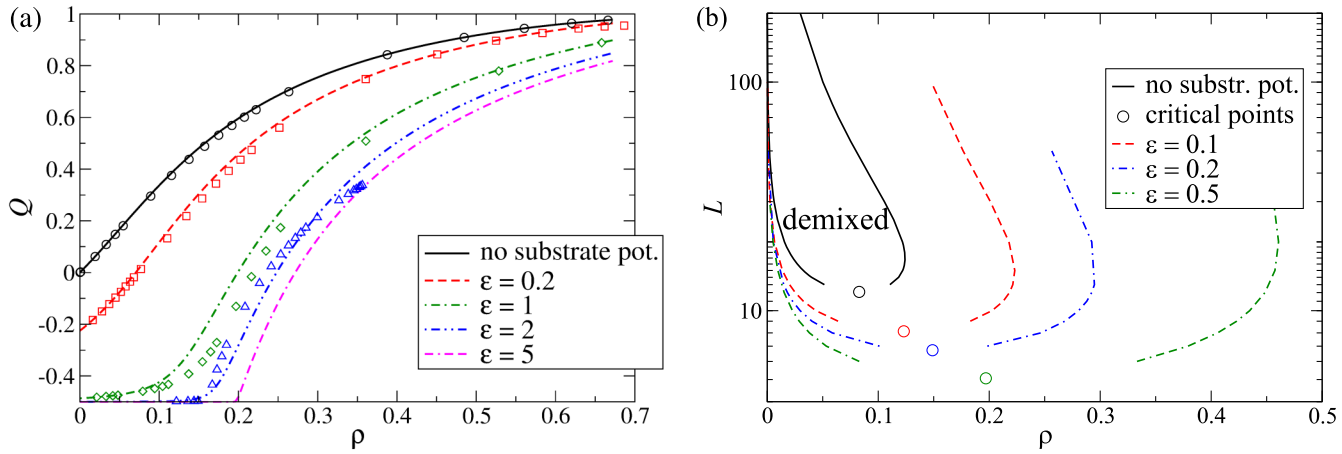

FIG. 5. (a) Order parameter Q for rods standing up vs. total density subject to a substrate potential (rod length $L = 5$). The substrate potential is parametrized as $-\epsilon$ per unit length such that $v_3 = -\epsilon$, $v_0 = -L\epsilon$ and thus $v_Q = (2/3)(L-1)\epsilon$. Lines are DFT results, symbols results from GCMC simulations (see Appendix A). The error is smaller than the symbol size. (b) FMT phase diagram (for nonzero substrate potential) showing the reentrant behavior for mixing ($S = 0$) and demixing ($S \neq 0$) in the plane. The critical points $\{L_c, \rho_c\}$ are located at $\{8.12, 0.123\}$ for $\epsilon = 0.1$, $\{6.72, 0.149\}$ for $\epsilon = 0.1$, and $\{5.06, 0.197\}$ for $\epsilon = 0.5$.

contribution) is obtained in the form $\rho(Q)$. For small deviations from equilibrium, $Q_{\rm eq} = Q_{\rm id} + \delta Q$, we can invert this function and obtain

$$\delta Q \approx \frac{3}{2}\rho \frac{\alpha - \beta Q_{\rm id}}{2(1+2Q_{\rm id})^{-1} + (1-Q_{\rm id})^{-1}}, \tag{40}$$

with $\alpha = 2(L^2 + L - 2)/9$ and $\beta = 2(L-1)^2/9$. Although the range of validity is very limited, it implies that the qualitative behavior for $\rho \to 0$ is unchanged since the slope of $\delta Q(\rho)$ is always positive. Thus the transition stays continuous. However, for increasing v_Q the "standing up" transition of the monolayer becomes increasingly steep at *moderate* densities; see Fig. 5(a) where we show the $Q(\rho)$ behavior for $L = 5$. For these moderate densities the expansion up to second order is no longer valid. Particularly for the case of $\epsilon = 5$ the behavior near $\rho = 0.2$ it appears $Q(\rho)$ has a bifurcation point, similar to the demixing transition in the 2D bulk system discussed in Sec. II C. The density $\rho = 0.2 = 1/L$ at which this apparent transition occurs is the close-packing density for rods lying flat. However, for finite potentials it is not a phase transition since $Q(\rho)$ maintains its linear behavior of $Q(\rho)$ with nonzero slope at very small densities.

A finite substrate potential has a marked influence on the reentrant transition for demixing in the plane. The location of the phase boundaries has been calculated using Eq. (35), with the condition $\mu_Q(\rho, Q_{\rm eq}, 0) = -\rho v_Q$ for $Q_{\rm eq}$. Fig. 5(b) shows the phase boundaries for the demixed phase with substrate potentials $\epsilon = 0.1$, 0.2, and 0.5 in comparison with the case $\epsilon = 0$. With increasing substrate potential, the density range for the demixed phase widens considerably and the critical point moves to smaller rod lengths.

III. MONOLAYERS OF HARD SPHEROCYLINDERS

For the lattice monolayer discussed in Sec. II it does not matter which rod point or segment is actually fixed to the plane since all choices lead to the same effective 2D model. Physically, fixing the end point corresponds to the case of rods on a hard substrate while fixing some other rod point (e.g., in the middle) applies to Langmuir monolayers. There should be a difference between the two cases which is not expected to be qualitative (with regard to the type of transition). As can be seen below, the low-density behavior of long rods with large aspect ratios is actually insensitive to the choice of confining plane. We thus present simulation results below solely for the case of fixed mid-points.

A. DFT in an expansion up to second order in density

We consider hard spherocylinders with length L and diameter D whose centers or ends are fixed on a plane. In order to investigate the nature of the orientation transition, we consider a low-density expansion of the free energy. This method was used for the well-studied model of hard rods in 3D to establish the onset of nematic order as a bifurcation and the nature as a first order transition.[28] The free energy density up to second order in density, including the contribution from an external potential, is given by

$$\mathcal{F} = \mathcal{F}^{\rm id} + \mathcal{F}^{\rm ex} + \mathcal{F}^{\rm ext}, \tag{41}$$

$$\mathcal{F}^{\rm id} = \int d^2r \int d\Omega\, \rho(\mathbf{r},\Omega)(\ln(\rho(\mathbf{r},\Omega)\Lambda^2) - 1), \tag{42}$$

$$\mathcal{F}^{\rm ex} = \frac{1}{2}\int d^2r \int d\Omega \int d^2r' \int d\Omega'\, \rho(\mathbf{r},\Omega) \times \rho(\mathbf{r}',\Omega')\omega(|\mathbf{r}-\mathbf{r}'|,\Omega,\Omega'), \tag{43}$$

$$\mathcal{F}^{\rm ext} = \int d^2r \int d\Omega\, \rho(\mathbf{r},\Omega)V^{\rm ext}(\mathbf{r},\Omega). \tag{44}$$

Here, $\rho(\mathbf{r},\Omega)$ is an inhomogeneous particle density in two dimensions and units of $[\text{length}]^{-2}$ which depends on the space point $\mathbf{r}$ and the orientation of the rod $\Omega = (\theta, \phi)$, specified by the polar angle θ and the azimuthal angle ϕ. The integral over orientations is defined as

$$\int d\Omega = \frac{1}{4\pi}\int_0^\pi \sin\theta d\theta \int_0^{2\pi} d\phi. \tag{45}$$

Λ is the thermal de Broglie length. $\omega(r,\Omega,\Omega')$ is the overlap function between rods for given orientations of and distance r between the particles. It is 1 if there is overlap, otherwise zero. The external (substrate) potential $V^{\text{ext}}(\mathbf{r},\Omega)$ is measured in units of k_BT.

We consider only orientation-dependent substrate potentials, $V^{\text{ext}}(\Omega)$, and bulk states, i.e., no spatial dependence of the density and introduce the orientation distribution $f(\Omega)$,

$$\rho(\mathbf{r},\Omega) = \rho_0 f(\Omega). \tag{46}$$

Then the ideal, excess, and external parts of the free energy per particle ($a = a^{\text{id}} + a^{\text{ex}} + a^{\text{ext}}$) become

$$a^{\text{id}} = \int d\Omega f(\Omega)(\ln(\rho_0\Lambda^2 f(\Omega)) - 1), \tag{47}$$

$$a^{\text{ex}} = \frac{\rho_0}{2}\int d\Omega \int d\Omega'\, f(\Omega)f(\Omega')\beta(\Omega,\Omega'), \tag{48}$$

$$a^{\text{ext}} = \int d\Omega\, f(\Omega)V^{\text{ext}}(\Omega). \tag{49}$$

Here, $\beta(\Omega,\Omega') = \int d^2r\omega(r,\Omega,\Omega')$ is the excluded area between the rod centers (or ends) with fixed orientations of the rods.

In equilibrium, $f(\Omega)$ minimizes a. From $\delta a/\delta f = 0$ we obtain

$$\ln f(\Omega) = -\ln C - V^{\text{ext}}(\Omega) - \rho_0 \int d\Omega'\, \beta(\Omega,\Omega')f(\Omega'), \tag{50}$$

where C is a constant ensuring that f is properly normalized, i.e., $\int d\Omega\, f(\Omega) = 1$. It is determined by exponentiating Eq. (50) and integrating over Ω,

$$\begin{aligned} f(\Omega) &= \frac{1}{C}\exp\left(-V^{\text{ext}}(\Omega) - \rho_0\int d\Omega'\, \beta(\Omega,\Omega')f(\Omega')\right), \\ C &= \int d\Omega \exp\left(-V^{\text{ext}}(\Omega) - \rho_0\int d\Omega'\, \beta(\Omega,\Omega')f(\Omega')\right). \end{aligned} \tag{51}$$

The orientation-dependent substrate potential gives rise to a non-constant orientational distribution in the ideal gas limit,

$$f_{\text{id}}(\Omega) = \frac{\exp(-V^{\text{ext}}(\Omega))}{\int d\Omega \exp(-V^{\text{ext}}(\Omega))}, \tag{52}$$

which is normalized to 1. We introduce the small deviation $f_1(\Omega) := f(\Omega) - f_{\text{id}}(\Omega)$ and linearize Eq. (51) in f_1,

$$\begin{aligned} \frac{f_1(\Omega)}{f_{\text{id}}(\Omega)} &= C_1 - \rho_0\int d\Omega'\beta(\Omega,\Omega')(f_{\text{id}}(\Omega') + f_1(\Omega')) \\ C_1 &= \rho_0\int d\Omega\int d\Omega' f_{\text{id}}(\Omega)\beta(\Omega,\Omega') \\ &\quad\times(f_{\text{id}}(\Omega') + f_1(\Omega')). \end{aligned} \tag{53}$$

The constant C_1 ensures the necessary normalization condition $\int d\Omega f_1(\Omega) = 0$. If one expands f_1 in powers of ρ_0, then one finds the leading order solution

$$\begin{aligned} f_1(\Omega) \approx \rho_0\, f_{\text{id}}(\Omega)\Bigg(&\int d\Omega\int d\Omega' f_{\text{id}}(\Omega)\beta(\Omega,\Omega')f_{\text{id}}(\Omega') \\ &- \int d\Omega'\beta(\Omega,\Omega')f_{\text{id}}(\Omega')\Bigg). \end{aligned} \tag{54}$$

This expression is equivalent to Eq. (40) in the lattice model and shows that any deviations from the ideal gas distribution are continuous and proportional to the density ρ_0.

In the absence of a substrate potential ($f_{\text{id}} = 1$), we can proceed further. Without loss of generality, we put rod 1 at the coordinate center with orientation (director) $\mathbf{u}_1 = (\sin\theta_1, 0, \cos\theta_1)^T$. Rod 2 has the director $\mathbf{u}_2 = (\sin\theta_2\cos\phi_2, \sin\theta_2\sin\phi_2, \cos\theta_2)^T$. The excluded area depends in general on the three angles $\theta_1, \theta_2, \phi_2$. If we consider only nematic order without biaxiality, $f(\Omega) \equiv f(\theta)$, then we can define the integrated overlap area

$$\frac{1}{2\pi}\int d\phi_2\beta(\theta_1,\theta_2,\phi_2) =: \beta_\phi(\theta_1,\theta_2). \tag{55}$$

If we take the polar angle (with respect to the interface normal) in the interval $[-\pi/2,\pi/2]$, symmetry considerations give us $\beta_\phi(\theta_1,\theta_2) = \beta_\phi(-\theta_1,\theta_2) = \beta_\phi(\theta_1,-\theta_2) = \beta_\phi(-\theta_1,-\theta_2)$. Since also $f(\theta) = f(-\theta)$, the integration domain over θ can be restricted to $[0,\pi/2]$. The nematic order parameter in the monolayer is defined by

$$Q_{\text{nem}} = \int_0^{\pi/2} d(\cos\theta)P_2(\cos\theta)\, f(\theta), \tag{56}$$

where $P_2(x)$ is the second of the Legendre polynomials $P_i(x)$. It is also useful to introduce the Legendre coefficients of the excluded area,

$$\begin{aligned} B_{ij} = &\int_0^{\pi/2} d(\cos\theta)P_{2i}(\cos\theta) \\ &\times\int_0^{\pi/2} d(\cos\theta')P_{2j}(\cos\theta')\, \beta_\phi(\theta,\theta'). \end{aligned} \tag{57}$$

Owing to the symmetry of the excluded area, projections only onto even Legendre polynomials are nonzero. Using these definitions, the nematic order parameter in the case of no substrate potential is obtained by projecting with P_2 onto the solution for f_1 in Eq. (54),

$$Q_{\text{nem}} \approx -\rho_0 B_{10}. \tag{58}$$

This is an interesting result since it tells us that $Q_{\text{nem}} \propto \rho_0$ as long as the leading off-diagonal Legendre coefficient of the excluded area is nonzero. This is precisely the case in the monolayer system (see below), whereas in 3D this coefficient vanishes. The linearity $Q_{\text{nem}} \propto \rho_0$ is completely equivalent to the linearity found in the lattice model in the absence of a substrate potential (see Eq. (37)).

The linearized equation (53) is connected to an approximated free energy per particle a_{lin} through $\delta a_{\text{lin}}/\delta f_1 = 0$. a_{lin} is quadratic in f_1 and is defined to give the difference to the isotropic state:

$$\begin{aligned} a_{\text{lin}} = &\frac{1}{2}\int_0^{\pi/2} d(\cos\theta)f_1(\theta)^2 + \frac{\rho_0}{2}\int_0^{\pi/2} d(\cos\theta) \\ &\times\int_0^{\pi/2} d(\cos\theta')\beta_\phi(\theta,\theta')(2 + f_1(\theta))f_1(\theta'). \end{aligned} \tag{59}$$

For the leading order solution (54), the free energy can be evaluated explicitly. It is convenient to use the Legendre expansion of the solution: $f_1 = \sum_{i=1}^{\infty} f_{1,i}P_{2i}(\cos\theta)$ with $f_{1,i} = -(2i+1)\rho_0 B_{i0}$. Using furthermore $B_{i0} = B_{0i}$ one finds

$$a_{\text{lin}} \approx -\frac{1}{2}\sum_{i=1}^{\infty}(2i+1)\rho_0^2 B_{i0}^2, \tag{60}$$

i.e., the free energy in the anisotropic state is always lower than in the isotropic state.

For hard spherocylinders in the limit $L/D \to \infty$ the excluded area does not depend on whether the rod centers or ends are fixed to the plane. Through geometric arguments (see Appendix B) we find

$$\begin{aligned}\beta(\theta_1,\theta_2,\phi_2) &= \frac{2LD}{\cos\theta_{\min}}|\sin\gamma|,\\ \theta_{\min} &= \min(|\theta_1|,|\theta_2|)\\ \cos\gamma &= \cos\theta_1\cos\theta_2 + \sin\theta_1\sin\theta_2\cos\phi_2,\end{aligned} \tag{61}$$

where γ is the angle between the rods. Thus we see that for long rods, a scaling $Q_{\text{nem}} \propto L\rho_0$ is predicted, which is different from $Q \propto L^2\rho$ found in the lattice model. The numerical evaluation of the Legendre coefficient in Eq. (58) gives

$$Q_{\text{nem}} \approx 0.45\ LD\rho_0 \qquad (L/D \to \infty). \tag{62}$$

B. Simulations

In order to validate the predictions from Sec. III A, we have performed Monte Carlo (MC) simulations of hard spherocylinders (cylinders of length L capped with two hemispheres of diameter D on either end) whose centers are restricted to move within a plane (off lattice) while the orientation vectors can take any direction in three-dimensional space. A cuboid simulation box with periodic boundary conditions and dimensions $L_x \times L_y \times (L+D)$ is used. Configurations have been generated using single particle displacement and rotations via the Metropolis scheme[29] as well as a specialized move for small densities that forces particles to come close to each other. We pick two random particles. If they are further apart than $(L+D)$, we move one into a circle of radius $(L+D)$ around the center of mass of the other. To fulfill detailed balance, the acceptance criterion of the inverse move (i.e., to remove one particle from the proximity of another and to place it somewhere in the plane) is simply multiplied by the ratio between the area of the simulation plane $(L_x \times L_y)$ and the area of that circle $(\pi(L+D)^2)$. We generated configurations for a fixed particle number N while varying the dimensions of the plane $L_x \times L_y$ to change the area number density of the rods ρ_0. After equilibration, we generated at least 10^6 independent configurations for each value of L/D, N, and ρ_0 to evaluate the nematic order parameter Q_{nem}.

At low densities, the simulations are subject to strong finite-size effects, which produce artefacts that might be misinterpreted as traces of a phase transition. In Fig. 6(a), we show $Q_{\text{nem}}(\rho_0)$ at low densities for two different N. Here, the horizontal lines mark the Q_{nem}-values obtained in simulations of freely penetrable rods. For an infinite number of particles, this value would be zero. However, since in the simulations we sum the orientational order tensor over a finite number of particles, its eigenvalues are not exactly zero and therefore the largest eigenvalue, corresponding to Q_{nem}, is always larger than zero. (This problem is not solved by the common strategy of taking twice the middle eigenvalue instead of the largest eigenvalue. It is inherent in the restriction to finite particle numbers.[31]) The horizontal lines thus mark the limit of detection of a Q_{nem} that truly signals orientational anisotropy for a given number of particles N. For a given N, there appears a first (lower) density above which orientational order is detectable, and a second (larger) density where the theoretically expected behavior $Q_{\text{nem}} \propto \rho_0$ sets in. These two densities are particle number dependent and shift towards zero with increasing N, and thus are not signatures of an additional phase transition. The solid line in Fig. 6(a) is the DFT result (Eq. (62)) derived in Sec. III A. For densities beyond the second density, the simulation results are very close to the DFT result and the density range where this occurs becomes larger with increasing system size.

The linearity $Q_{\text{nem}} \propto \rho_0$ can also be seen in numerical results for a monolayer of ellipsoids[14] (Fig. 4 therein, for an aspect ratio of 10). The density functional used in Ref. 14 reduces to Eq. (43) in the low-density limit and should therefore comply with the present analysis; however, explicit expressions have not been given in Ref. 14. Corresponding Monte Carlo simulation results in Ref. 14 show agreement with the DFT results but low densities have not been considered.

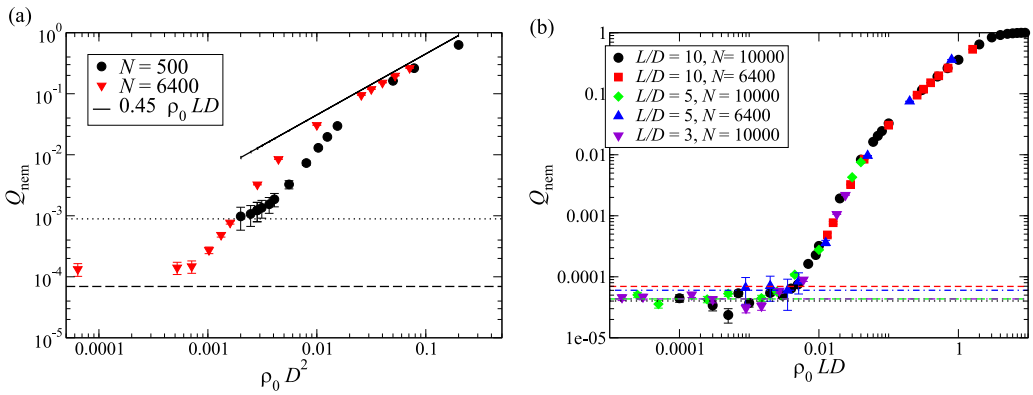

FIG. 6. (a) Finite system size analysis, rod length $L/D = 10$. The dashed and dotted horizontal lines are Q_{nem} values obtained for a system of freely penetrable rods for particle numbers $N = 6400$ and 500, respectively, while the solid line is the DFT result (Eq. (62)). (b) Order parameter Q_{nem} vs. $\rho_0(L/D)$ plot for different aspect ratios L/D and numbers of rods N. The horizontal lines are as in (a).

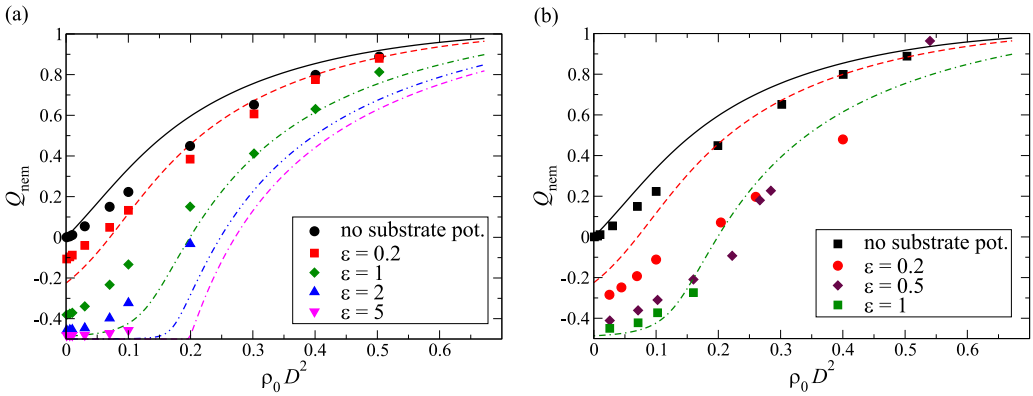

FIG. 7. Order parameter Q_{nem} vs. number density $\rho_0 D^2$ for rods subject to an attractive substrate potential ($L/D = 5$). The dashed lines are the results from the lattice model shown in Fig. 5 while data points correspond to the off-lattice simulation (errors smaller than symbol size). The substrate potential is orientation-dependent defined by (a) $V^{\text{ext}} = -\epsilon(L/D)\sin\theta$ and, (b) $V^{\text{ext}} = -\epsilon(L/D)\sin^2\theta$, where θ is the angle between rod director and the substrate normal.

In Fig. 6(b), we show Q_{nem} vs. $\rho_0(L/D)$, which is independent of the aspect ratio L/D. System sizes are very similar here such that the finite size effect discussed above is not visible.

In the presence of an attractive substrate potential, we qualitatively observe the same behaviour as in the lattice model (see Fig. 7). We compare two different potentials (a) $V^{\text{ext}} = -\epsilon(L/D)\sin\theta$ and, (b) $V^{\text{ext}} = -\epsilon(L/D)\sin^2\theta$, where θ is the angle between rod director and the substrate normal. Both choices drive the system toward nematic order (rods "standing up"), with choice (b) the external free energy per particle (Eq. (49)) becomes

$$a^{\text{ext}} = \int_0^{\pi/2} d\theta\ f(\theta) V^{\text{ext}}(\theta) = \frac{2}{3}\,\epsilon\,\frac{L}{D}\,(Q_{\text{nem}} - 1). \quad (63)$$

Similar to the choice of the external potential in the lattice model (Eq. (38)), the corresponding free energy contribution (apart from an additive constant) is proportional to the nematic order parameter. The plots show qualitative agreement with the lattice model as Q_{nem} remains continuous and the "standing up" transition becomes steeper with increasing substrate potential parameter ϵ.

For the moderate aspect ratios investigated here (between 3 and 10 in the case of no substrate potential and 5 for the attractive substrate) no transition to a biaxial state has been found. Such a biaxial state would correspond to the demixing in the plane investigated in the lattice model. In Ref. 14, the biaxial transition was investigated in more detail for their system of ellipsoids on a plane and an effective substrate attraction mimicked by a restriction of the polar angle to values between a nonzero limiting angle and $\pi/2$. Using DFT, the authors find that the occurrence of a biaxial transition is very sensitive to the limiting angle: for zero angle (no substrate potential) no transition has been found for aspect ratios up to 20 whereas small nonzero angles induce this transition.

IV. SUMMARY AND DISCUSSION

In this paper, we have analyzed the equilibrium properties of hard rod monolayers by employing density functional theory and Monte Carlo simulations for a cubic lattice model (resulting in restricted translational and orientational degrees of freedom for the rods) and a continuum model with hard spherocylinders (having unrestricted in-plane translational and orientational degrees of freedom). We used lattice fundamental measure theory as a DFT for the lattice model. In two and three dimensional bulk systems, lattice FMT predicts rod demixing and a first order nematic transition, respectively. Applied to the monolayer situation, lattice FMT shows a continuous "standing-up" transition of the rods with increasing density. These results are in excellent agreement with our results from GCMC simulations. For the continuum model, the same type of continuous "standing-up" transition is predicted by DFT in a virial expansion. In MC simulations, the transition is masked by strong finite-size effects but we have evidence that for large system sizes simulations and DFT agree. Although the transitions in the lattice and the continuum model are very similar, there is a qualitative difference in the scaling with the rod extension (at low densities ρ). The lattice model does not show a simple scaling of the nematic order with respect to a scaled density variable whereas in the continuum model the scaling is with ρLD, where L and D are length and diameter of the rods. This can be understood from the scaling of the second virial coefficient.

The presence of an attractive surface potential does not change the continuous character of the "standing-up" transition. However, for attractive energies per unit rod length which are of the order of 5 $k_{\text{B}}T$ or larger, the transition resembles a second order transition as present, for instance, in the bulk 2D system.

Our results are a first step towards modelling the equilibrium and growth of thin films with anisotropic particles with simple coarse-grained models. Investigations of the dynamics of monolayer growth with hard rods would be the logical next step.[30] Incorporating particle attractions as well as extending the investigations to multiple layers is desirable and should be pursued both by equilibrium and growth investigations in order to clarify the influence of the equilibrium phase diagram vs. purely kinetic effects onto the final structures.

ACKNOWLEDGMENTS

This work is supported within the DFG/FNR INTER project "Thin Film Growth" by the Deutsche Forschungs-

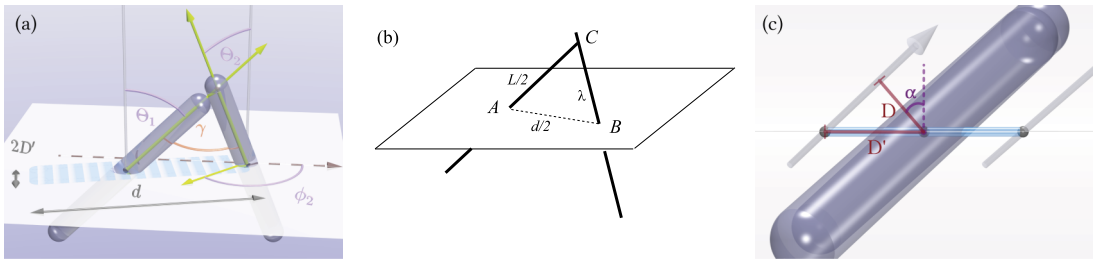

FIG. 8. (a) and (b) Hard rods (spherocylinders) with their mid-points fixed on the substrate plane. The area enclosed in dashed lines is the excluded area and can be approximated by a rectangle with side lengths d and D' in the limit $L/D \to \infty$. (c) Side view on the two hard rods from a perspective where rod 2 is exactly hidden behind rod 1.

gemeinschaft (DFG), Project No. OE 285/3-1 by the Fonds National de la recherche (FNR) Luxembourg, and by the Landesgraduiertenförderung Baden-Württemberg. Data from computer simulations presented in this paper were produced using the HPC facilities of the University of Luxembourg.[32] The authors acknowledge stimulating discussions with Frank Schreiber.

APPENDIX A: EQUILIBRIUM GRAND-CANONICAL SIMULATIONS FOR THE MONOLAYER IN THE LATTICE MODEL

The simulation results for the lattice monolayer system were obtained using grand canonical Monte Carlo (GCMC) simulations on an $M \times M$ lattice. We treated the rods with a fixed orientation as a distinct species with corresponding particle number N_i ($i = 1 \ldots 3$). The chemical potential μ was equal for all three species. In each GCMC step, insertion or deletion of a rod was chosen with probability 1/2. Then, the species on which the insertion/deletion is performed was chosen with probability 1/3. For the insertion move $N_i \to N_i + 1$, a random lattice site was chosen. If no overlap with the existing rods occurs, the move was accepted with probability $\alpha_{\text{ins}} = \min\left(1, M^2/(N_i+1)\, z\, \exp(-\Delta V^{\text{ext}})\right)$, where $z = \exp(\mu/(k_B T))$ and ΔV^{ext} is the change in external energy upon insertion of the rod. For the deletion move $N_i + 1 \to N_i$, a particle from species i was chosen randomly and removed with probability $\alpha_{\text{del}} = \min\left(1, (N_i+1)/M^2\, z^{-1}\, \exp(+\Delta V^{\text{ext}})\right)$.

We used lattices with $M = 256$ and 10^7 single moves for a data point with no or small external potential. For stronger external potentials, we used 10^8 moves ($\epsilon = \{1, 2\}$).

APPENDIX B: EXCLUDED AREA FOR HARD SPHEROCYLINDERS IN THE LIMIT *L/D* → ∞

Here we briefly derive Eq. (61). The geometric definitions are given in Fig. 8. For infinitely thin hard rods, the (maximum) distance of closest approach $d/2$ is given by

$$d/2 = \frac{(L/2)}{\cos\theta_{\min}} \sqrt{\cos^2\theta_1 + \cos^2\theta_2 - 2\cos\theta_1 \cos\theta_2 \cos\gamma}. \tag{B1}$$

This is obtained from the law of cosines in the triangle ABC (see Fig. 8(b)) where $\lambda = (L/2)\cos\theta_{\max}/\cos\theta_{\min}$ and $\theta_{\min[\max]} = \min[\max](|\theta_1|, |\theta_2|)$. If we now consider a finite, small thickness D of the rods then rod 2 may slide past rod 1 at a distance D' to either side of rod 1 along the direction of d. This defines the excluded area (enclosed in dashed lines in Fig. 8(a)). It is a rectangle with side lengths d and $2D'$. According to Fig. 8(c), the distance D' is given by

$$D' = \frac{D}{\sin\alpha}, \tag{B2}$$

where α is the angle of $\mathbf{e}_z$ with the normal vector $\mathbf{n}$ to the plane spanned by the two rods. This normal vector is given by

$$\mathbf{n} = \frac{\mathbf{u}_1 \times \mathbf{u}_2}{|\sin\gamma|}, \tag{B3}$$

where $\mathbf{u}_i$ is the normalized director of rod i. Thus

$$\cos\alpha = \mathbf{n} \cdot \mathbf{e}_z = \frac{\sin\theta_1 \sin\theta_2 \sin\phi_2}{|\sin\gamma|}. \tag{B4}$$

Insertion into Eq. (B2) and some manipulations give

$$D' = D\, \frac{|\sin\gamma|}{\sqrt{\cos^2\theta_1 + \cos^2\theta_2 - 2\cos\theta_1 \cos\theta_2 \cos\gamma}}, \tag{B5}$$

such that finally the excluded area becomes

$$\beta(\theta_1, \theta_2, \phi_2) \approx 2D'd = \frac{2LD}{\cos\theta_{\min}} |\sin\gamma|. \tag{B6}$$

[1]V. M. Kaganer, H. Möhwald, and P. Dutta, Rev. Mod. Phys. **71**, 779 (1999).
[2]F. Schreiber, Prog. Surf. Sci. **65**, 151 (2000).
[3]F. Schreiber, Phys. Status Solidi A **201**, 1037 (2004).
[4]G. Witte and C. Wöll, J. Mater. Res. **19**, 1889 (2004).
[5]Y. Rosenfeld, Phys. Rev. Lett. **63**, 980 (1989).
[6]H. Hansen–Goos and K. Mecke, Phys. Rev. Lett. **102**, 018302 (2009).
[7]L. Lafuente and J. A. Cuesta, J. Phys.: Condens. Matter **14**, 12079 (2002).
[8]L. Lafuente and J. A. Cuesta, Phys. Rev. Lett. **93**, 130603 (2004).
[9]R. van Roij, M. Dijkstra, and R. Evans, J. Chem. Phys. **113**, 17 (2000).
[10]Y. Martinez-Raton, Phys. Rev. E **69**, 061712 (2004).
[11]B. S. John, C. Juhlin, and F. A. Escobedo, J. Chem. Phys. **128**, 044909 (2008).
[12]Y. Martinez-Raton, S. Varga, and E. Velasco, J. Chem. Phys. **140**, 204906 (2014).
[13]M. Gonzalez-Pinto, Y. Martinez-Raton, E. Velasco, and S. Varga, Phys. Chem. Chem. Phys. **17**, 6389 (2015).
[14]S. Varga, Y. Martinez-Raton, E. Velasco, G. Bautista–Carbajal, and G. Odriozola, Phys. Chem. Chem. Phys. **18**, 4547 (2016).
[15]T. K. Vanderlick, H. T. Davis, and J. K. Percus, J. Chem. Phys. **91**, 7136 (1989).
[16]B. Bakhti, S. Schott, and P. Maass, Phys. Rev. E **85**, 042107 (2012).
[17]T. Fischer and R. L. C. Vink, EPL **85**, 56003 (2009).
[18]A. Ghosh and D. Dhar, EPL **78**, 20003 (2007).

[19]D. H. Linares, F. Roma, and A. J. Ramirez-Pastor, J. Stat. Mech.: Theory Exp. **2008**, P03013.
[20]D. A. Matoz-Fernandez, D. H. Linares, and A. J. Ramirez-Pastor, J. Chem. Phys. **128**, 214902 (2008).
[21]J. Kundu, R. Rajesh, D. Dhar, and J. F. Stilck, Phys. Rev. E **87**, 032103 (2013).
[22]J. Kundu and R. Rajesh, Phys. Rev. E **89**, 052124 (2014).
[23]J. Kundu and R. Rajesh, Eur. Phys. J. B **88**, 133 (2015).
[24]J. Kundu and R. Rajesh, Phys. Rev. E **91**, 012105 (2015).
[25]A. M. Luo, L. M. C. Sagis, and P. Ilg, J. Chem. Phys. **140**, 124901 (2014).
[26]P. Bolhuis and D. Frenkel, J. Chem. Phys. **106**, 666 (1997).
[27]D. Kramer, A. Ben-Shaul, Z.-Y. Chen, and W. M. Gelbart, J. Chem. Phys. **96**, 2236 (1992).
[28]R. F. Kayser, Jr. and H. J. Raveche, Phys. Rev. A **17**, 2068 (1978).
[29]N. Metropolis, A. W. Rosenbluth, M. N. Rosenbluth, A. H. Teller, and E. Teller, J. Chem. Phys. **21**, 1087 (1953).
[30]M. Klopotek, H. Hansen–Goos, M. Dixit, T. Schilling, F. Schreiber, and M. Oettel, "Monolayers of hard rods on planar substrates: II. Growth" (unpublished).
[31]R. Eppenga and D. Frenkel, Mol. Phys. **52**, 1303–1334 (1984).
[32]S. Varrette, P. Bouvry, H. Cartiaux, and F. Georgatos, in *Proceedings of the 2014 International Conference on High Performance Computing and Simulation (HPCS 2014)* (IEEE, Bologna, Italy, 2014), pp. 959–967.